

EPR Investigation of TiCl_3 Dissolved in Polar Solvents. Implications for the Understanding of Active Ti(III) Species in Heterogeneous Ziegler-Natta Catalysts.

Sara Maurelli,^{a,c} Elena Morra,^{a,b,c} Sabine Van Doorslaer,^{*a} Vincenzo Busico,^d Mario Chiesa^{*b}

^{a)} *University of Antwerp, Department of Physics, Universiteitsplein 1, B-2610 Wilrijk, Belgium*

^{b)} *Dipartimento di Chimica, University of Torino Via Giuria, 7 - 10125 Torino, Italy.*

^{c)} *Dutch Polymer Institute (DPI), P.O. Box 902, 5600 AX Eindhoven, The Netherlands.*

^{d)} *Dipartimento di Scienze Chimiche, Università degli Studi di Napoli Federico II, Via Cintia, 80126 Napoli, Italy.*

E-mail: sabine.vandoorslaer@uantwerpen.be, mario.chiesa@unito.it

SUPPORTING INFORMATION

1) EPR spectrum of α -TiCl₃ and (b) β -TiCl₃ powders

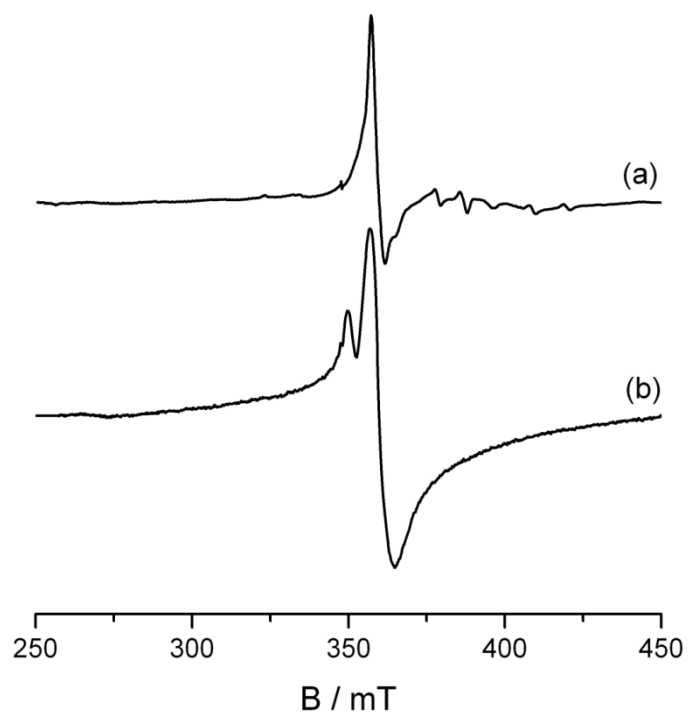


Figure S1. Experimental X-band CW EPR spectra of (a) α -TiCl₃ and (b) β -TiCl₃ powders recorded at $T = 10\text{K}$. The spectral intensities are normalized.

2) EPR spectrum of TiCl_3 dissolved in anhydrous methanol

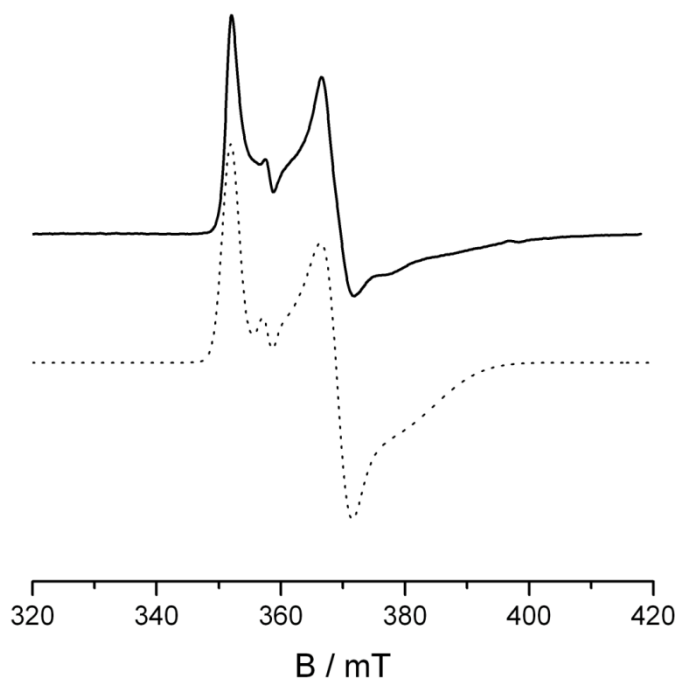


Figure S2. Experimental (solid line) and computer simulation (dotted line) X-band CW EPR spectrum of TiCl_3 dissolved in anhydrous methanol. The parameters extracted from the computer simulation are listed in Table 1 of the main text. In the simulation the ^{47}Ti and ^{49}Ti hyperfine couplings obtained from DFT modelling (Table S1) are taken into account. We remark that given the low natural abundance of the magnetically active Ti isotopes (^{47}Ti and ^{49}Ti) and the relatively broad line width of the experimental spectrum, the Ti-hyperfine tensors are not actually resolved in the experiment.

Table S1. DFT-computed ^{47}Ti hyperfine tensors for the complexes illustrated in Figure 4 of the main text. All hfi and nqi values are in MHz, while Euler angles are in degree. The values of complex b have been used for the simulation reported in Figure S2.

Complex	A_x	A_y	A_z	α, β, γ
a	18.9	21.7	68.4	30.1, 35.1, 14.1
b	24.9	67.7	15.8	-29.6, 19.4, 26.2
c	28.8	78.1	26.7	-26.0, 26.4, -66.1
d	18.8	68.5	18.3	-18.9, 0.6, -84.4
e	28.7	78.6	27.1	-35.0, 29.2, -60.5
f	19.8	72.7	24.6	-3.7, 4.2, -96.5

3) Field-dependent 2-pulse ESEEM experiments

The different local geometry and/or nature of the first coordinating ligands can be expected to influence the relaxation times of the two different species. In order to check this hypothesis the two-pulse echo decay was detected as a function of the resonant magnetic field. In this way the echo-detected EPR spectrum can be obtained and the T_2 relaxation time can be used to filter off spectral components associated to fast relaxing species, allowing, in principle, to isolate the two overlapping spectra. The results of the experiment are shown in Figure S3.

The experiment indicates that the overall absorption pattern depends on the inter-pulse τ delay, suggesting the presence of species with slightly different phase memory time (T_m). T_m measured at the top of the echo intensity ($B=355$ mT coinciding with species 2) is of the order of 200 ns, while at $B=375$ mT (coinciding with the maximum absorption of species 1) a value of 250 ns is recorded. These values, although different, do not allow the deconvolution of the spectrum and clear determination of the single contributing species.

The spectra of the two species can however be distinguished from each other by plotting the resonant magnetic field as a function of the ESEEM frequencies obtained after Fourier transformation of the spectrum in the time dimension. The result is shown in Figure S4, where the 2D spectrum shows the presence of features at 15MHz due to coordinated protons ($\nu_H=14.98$ MHz) and in the low frequency region presumably associated to the presence of $^{35,37}\text{Cl}$ ligands. In particular, a relatively broad peak is present at approximately 5 MHz, which can be associated to the presence of coordinated chloride ions (*vide infra*) are clearly identified. By plotting the 5 MHz and 15 MHz ESEEM frequencies as a function of the resonant magnetic field the EPR spectrum associated to two species characterized by the presence of coordinated protons (methanols) and Cl nuclei can clearly be distinguished.

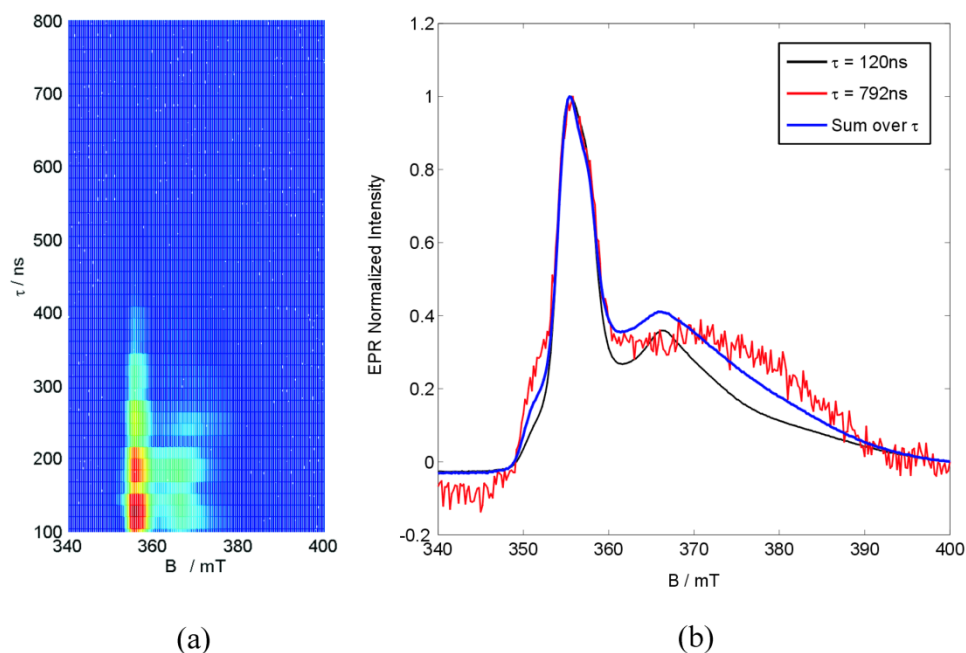


Figure S3. Experimental 2D ESE detected spectra recorded at different time delay τ of the pulse sequence: $t_{\pi/2} - \tau - t_{\pi} - \tau - echo$, with $t_{\pi/2} = 16$ ns and $t_{\pi} = 32$ ns. (a) Echo decay spectra recorded at different τ values (350 τ values starting from 88 ns with $\Delta\tau = 16$ ns) within a magnetic field sweep of 60 mT (from $B = 340$ mT to $B = 400$ mT). (b) ESE-detected EPR spectra recorded at $\tau = 120$ ns (black line), $\tau = 792$ ns (red line) and ESE spectrum as resulting from the sum over the 350 τ values (blue line).

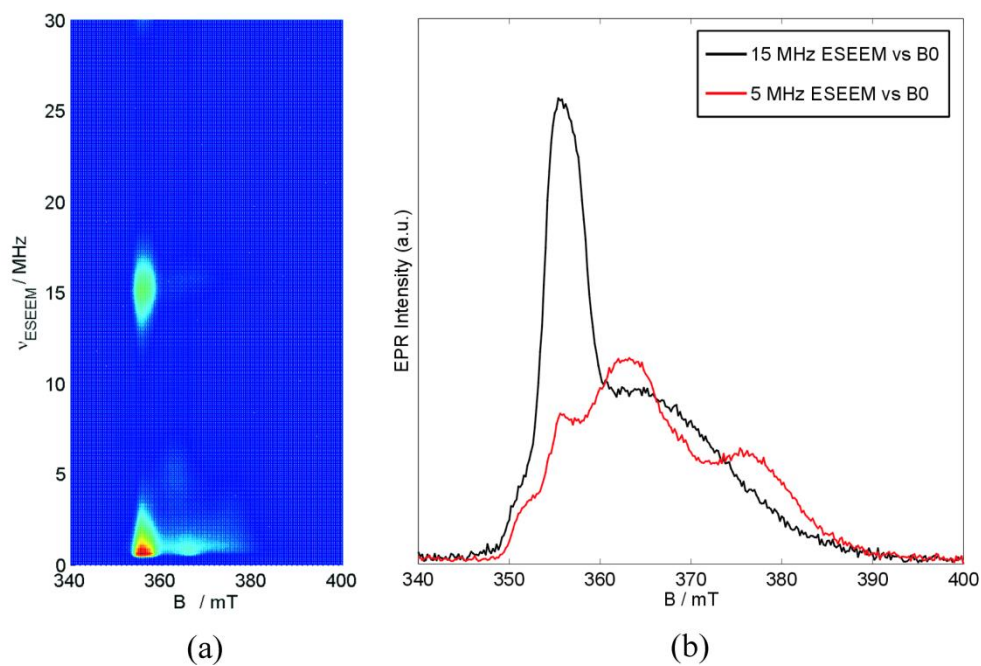


Figure S4. Experimental 2D ESE-detected spectra recorded at different time delay τ of the pulse sequence: $t_{\pi/2} - \tau - t_{\pi} - \tau - \text{echo}$, with $t_{\pi/2} = 16\text{ns}$ and $t_{\pi} = 32\text{ns}$. (a) Echo decay spectra upon Fourier transformation recorded at different τ values (350 τ values starting from 88ns with $\Delta\tau = 16\text{ns}$) and plotted in the ESEEM frequencies domain versus the magnetic field sweep of 60mT (from $B = 340\text{mT}$ to $B = 400\text{mT}$). (b) Field spectra corresponding to the ESEEM frequencies $\nu_{\text{ESEEM}} = 15\text{MHz}$ (black line) and $\nu_{\text{ESEEM}} = 5\text{MHz}$ (red line).

4) Evolution of the EPR spectrum as a function of TiCl_3 concentration in the water-methanol solution

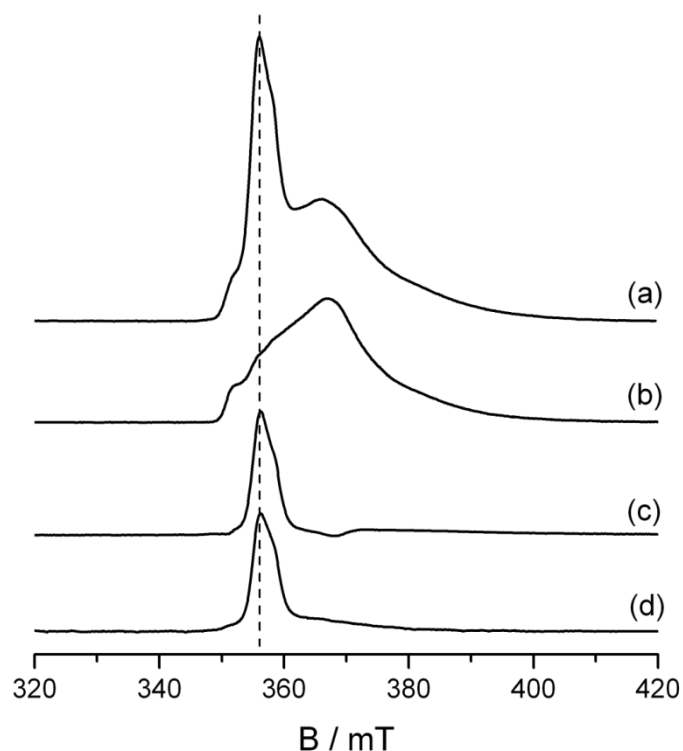


Figure S5. Experimental X-band ESE-detected EPR spectra of frozen solutions of (a) TiCl_3 dissolved in hydrated methanol, (b) anhydrous methanol, (c) subtraction of the spectra (a) - (b), (d) diluted TiCl_3 -hydrated methanol solution (hence with increased water/Ti(III) ratio). The spectra were recorded at $T = 10\text{K}$. The difference in the experimental microwave frequency was taken into account when subtracting the spectra. The spectra are all shown rescaled for the same microwave frequency.

5) HYSORE Simulations

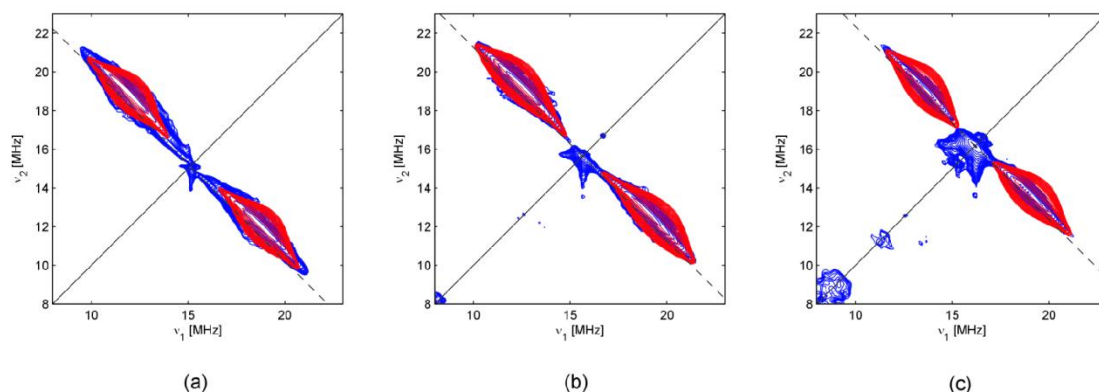


Figure S6. Experimental (blue line) and computer simulation (red line) ^1H HYSORE spectra of TiCl_3 dissolved in hydrated methanol water recorded at $\tau = 128\text{ns}$ and observer positions (a) $B_0 = 355.0\text{ mT}$, (b) $B_0 = 367.3\text{ mT}$ and (c) 380.0 mT . The parameters extracted from the computer simulations are listed in Table 2 of the main text. The same proton couplings have been observed for the anhydrous methanol solution.

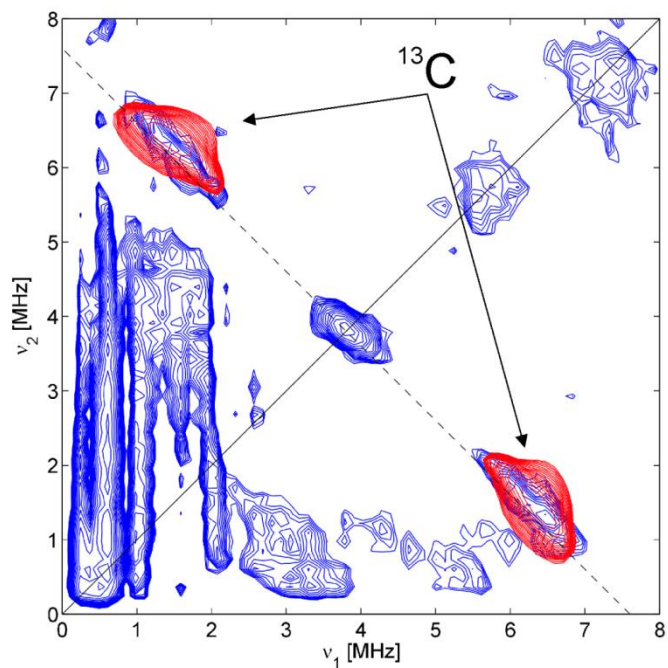


Figure S7. Experimental (blue line) and computer simulation (red line) ^{13}C HYSCORE spectrum of TiCl_3 dissolved in hydrated methanol. The spectrum is taken at $B_0 = 355.0$ mT and $\tau = 128$ ns. The parameters extracted from the computer simulations are listed in Table 2 of the main text.

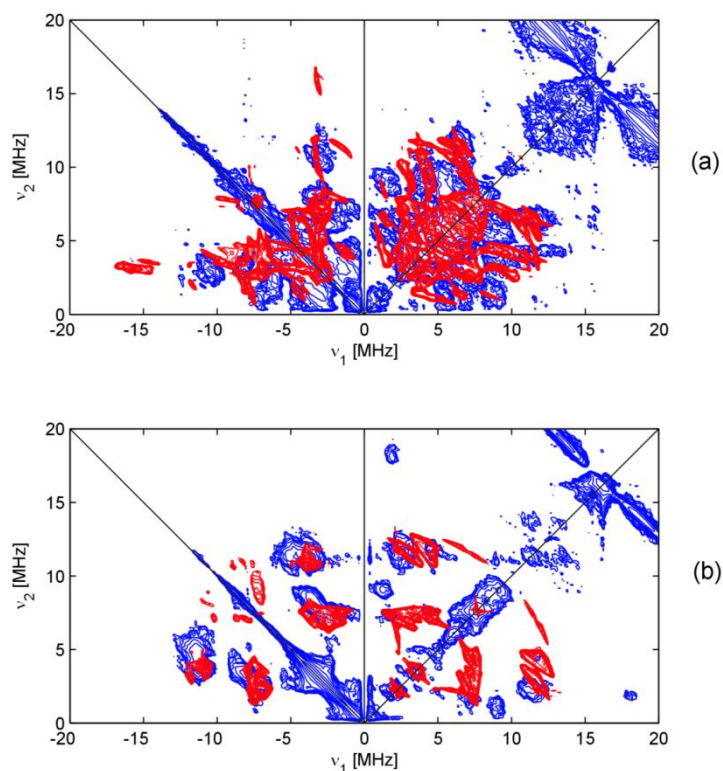


Figure S8. Experimental (blue line) and computer simulation (red line) $^{35,37}\text{Cl}$ HYSCORE spectra of TiCl_3 dissolved in anhydrous methanol recorded at $\tau = 128$ ns and observer positions (a) $B_0 = 367.3$ mT and (b) $B_0 = 380.0$ mT. The computer simulations, whose parameters are listed in Table 2, consider the interaction of the unpaired electron with one chlorine nucleus. To account for all cross peaks including those involving combination frequencies, different chlorine nuclei should be taken into account, as well as the contributions of the protons.

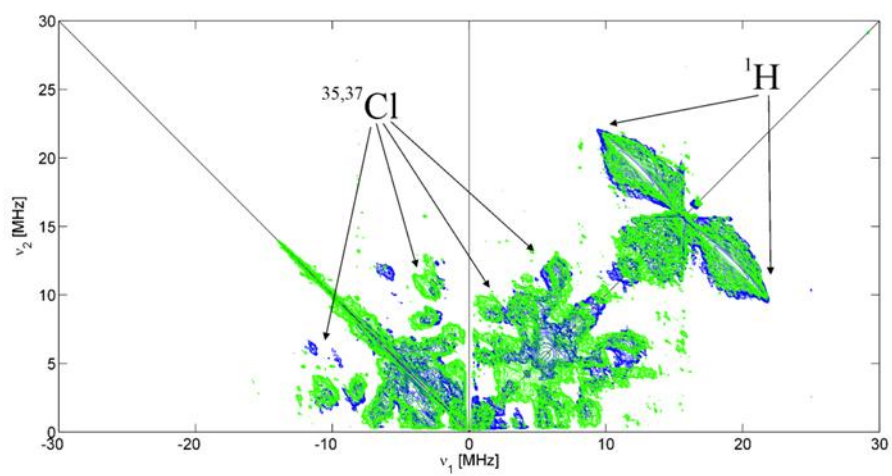


Figure S9. Experimental X-band HSCORE spectra of TiCl_3 dissolved in hydrated (blue line) and anhydrous (green line) methanol recorded at $B_0 = 365.0$ mT and $\tau = 128$ ns. The identity of the two spectra reassures that under both conditions (hydrated and anhydrous methanol solutions) the same species are present.